Handling Large Power Steps in Real-Time Microgrid Control via Explicit Power Setpoints

Roman Rudnik
Jean-Yves Le Boudec
Andrey Bernstein
Laboratory for Communications and Applications 2
École Polytechnique Fédérale de Lausanne
Lausanne, Switzerland
{roman.rudnik, jean-yves.leboudec, andrey.bernstein}@epfl.ch

Lorenzo Reyes-Chamorro
Mario Paolone
Distributed Electrical Systems Laboratory
École Polytechnique Fédérale de Lausanne
Lausanne, Switzerland
{lorenzo.reyes, mario.paolone}@epfl.ch

***Abstract*—We consider a microgrid with real-time control using explicit power-setpoints. Sudden power-steps, such as load disconnections or load in-rushes, directly affect the decisions of the microgrid controller that aims at avoiding voltage or line-ampacity violations. When trying to completely avoid these violations, the grid operation may be too restricted, which may lead to large suboptimality. However, temporary violations of the steady-state bounds are allowed by grid standards and could enable the exploitation of the flexibility of other resources to better control the system's state. In this paper, we propose a method by which such temporary violations are controlled so that they remain within the limits imposed by grid standards and safe operation. The method is experimentally tested and validated on a real microgrid.**

***Index Terms*—Real-time control, power steps, microgrid, explicit power-setpoints, soft operational-constraints.**

I. Introduction

Recently, the number of high-power energy resources in distribution grids, such as electric vehicles (EV), is growing rapidly. These loads could represent the largest ones in microgrids, having a non-negligible impact on their operation. Indeed, the sudden connection or disconnection of such resources may heavily impact the operation of the electrical grid. Specifically, the two major challenges related to distribution systems operation are voltage control and lines congestion management. Possible solutions are grid reinforcement, advanced droop control or real-time agent based control. In this paper we are interested in the last solution.

As an example, consider a grid-tied microgrid, that contains local generation (PV or storage system) and electric vehicle charging stations. When an EV suddenly disconnects (e.g., by decision of the EV user) a large power step occurs, potentially leading to overvoltages or overcurrents[1] caused by the local generation that was absorbed by the EV before the step. With real-time agent-based controls, possible solutions might curtail local generation or reduce the EV charging power prior to the step, thus enabling the grid to be always prepared for the large power step.

However, hardly defined operational limits can be violated for short amounts of time with no harm to the grid. For instance, for voltage violations, electric standards (such as [1]) define time-dependent operational bounds. For maximum currents on power lines, line ampacities[2] are typically not violated. However, the actual operational constraint of a line is its conductor temperature [2]. The line can therefore be temporarily and safely overloaded[3]; the limit depends on *specific energy* characteristic [3].

In this paper, we propose a method that allows a real-time grid controller to continuously provide optimal control by relaxing the pre-defined hard constraints and allowing temporary voltage and current violations. More precisely, we make use of the specific real-time control framework in COMMELEC [4] and modify the decision process of the grid controller (a.k.a grid agent), by defining state-dependent penalty functions in the optimization process. We evaluate our proposed solution using a real scale microgrid equipped with real loads, distributed generators and storage. To the best of our knowledge, this is the first attempt to design a real-time grid controller that accounts for temporary voltage and current violations according to electric standards.

The structure of this paper is the following. Section II briefly describes the COMMELEC framework. In Section III, we focus on the details of the proposed methodology. Finally, Section IV provides the results of the experimental validation of the method on a real microgrid.

II. The Commelec Framework

COMMELEC is multi agent-based framework for real-time control of an electrical grid. The agents are responsible for an entire grid (Grid Agent - GA) or for single resources (Resource Agents - RA [5]).

The GA communicates with its RAs using a common, device-independent protocol for message exchange. More precisely, each RA advertises an abstract representation of its internal state using the following format: (1) The PQ *profile* is the set in the (P, Q) plane (for active and reactive power) that the resource under the control of the RA can deploy.

[1] In this paper we do not consider electromagnetic transients.

[2] also known as Permanently Admissible Tramission Loading: PATL

[3] known as Temporarily Admissible Tramission Loading: TATL

(2) The *virtual cost* $C(P,Q)$ is a function, that evaluates the preference of a system to stay in a particular zone of the PQ *profile*. (3) The *belief function* $BF(P,Q)$ is a set valued function that accounts for the uncertainty of the resource operation. Specifically, it returns a convex set that contains all possible set-points that the resource might implement when it is instructed to apply (P,Q).

The main goal of the GA is to steer the electrical state of its grid in real-time by explicitly setting the power setpoints so that the grid is in a feasible state of operation, that is, the nodal voltage magnitudes and line currents are in safe bounds. To perform this, the GA first needs the advertisements from the resources and the estimation of the current electrical state of the grid. Then the GA computes optimal power setpoints, using a gradient-based method, and sends them to RAs. These process is repeated every 100ms. Thus, the GA has a software-based delay in the sense that it cannot control the grid between two consecutive time-steps. However, the GA makes sure that the state of the grid will be feasible during the next 100 ms by estimating the maximum variation of control using the belief functions. For instance, for EVs, which can be disconnected at any moment, the belief function should take into account the fact that the power consumption might be suddenly equal to zero. Therefore, the advertised belief function is equals to $BF(P) = [-P, 0]$ (assuming reactive power $Q = 0$).

III. Penalty Functions in the Grid Agent

As already mentioned, the main task of the GA is to compute setpoints for each RA. To do so, the GA attempts to minimize an objective function that integrates the virtual costs of the resources and a penalty term J that is used to keep voltages and currents between admissible bounds. Let us denote the penalty term for voltage as J_V and penalty term for current as J_I, so that $J = J_V + J_I$. In [4] these functions are chosen as follows (in the next subsection, we propose a suitable modification of these functions):

$$J_V = \sum_k J_{V,k}(V_k) \tag{1}$$

where

$$\begin{aligned} J_{V,k}(V_k) &\triangleq \frac{(V_k - V_k^{nom})^2}{\beta_k^2 - (V_k - V_k^{nom})^2} \\ &\quad \text{if } V_k \in [V_k^{nom} - \beta_k, V_k^{nom} + \beta_k] \\ &= \infty \text{ otherwise, and} \end{aligned} \tag{2}$$

$$\begin{aligned} J_I &= \sum_l \frac{I_l^2}{(I_l^{max})^2 - I_l^2} \text{ if } I_l \le I_l^{max} \\ &= \infty \text{ otherwise.} \end{aligned} \tag{3}$$

In the above β_k (typically 10% of the nominal voltage) and I_l^{max} are threshold variables, V_k is the voltage magnitude at bus k and V_k^{nom} its nominal value. I_l is the current magnitude at a line l. In other words, the original penalty functions introduce hard constraints on voltages and currents.

A. Modification to the Voltage Penalty-Function

The standard [1] claims that an undervoltage of 30% and an overvoltage of 20% of the nominal voltage are allowed for at most $T_v = 500$ms. We call T_v the *violation period*. To account for this, we first replace the hard constraints involving β_k in Eq. (2) by

$$V_k \in [V_k^{nom} - \underline{\gamma}_k, V_k^{nom} + \bar{\gamma}_k] \tag{4}$$

where $\underline{\gamma}_k, \bar{\gamma}_k > \beta_k$ represent the 20% overvoltage and 30% undervoltage bounds respectively. We also define the *relaxation period* T_r, as the time-window that should elapse between two-consecutive violations periods. Note that standards do not explicit such a period. However, in our understanding, a relaxation period of several minutes is necessary in order to avoid repetitive violations. In this paper, we take $T_r = 3$min.

Second, we define four states, that indicate whether the bus is in relaxation or violation period, as defined below:

States	I	II	III	IV
in relaxation ($\tau_{r,k} < T_r$)	No	No	Yes	Yes
in violation ($\tau_{v,k} < T_v$)	No	Yes	Yes	No

where timers $\tau_{r,k}$ and $\tau_{v,k}$ count the time that a bus k is in relaxation or violation period respectively. Fig. 1 shows the associated state-machine.

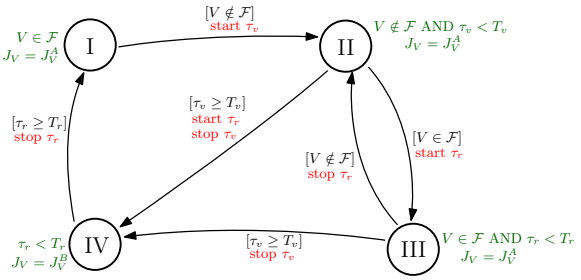

Fig. 1: States transitions per bus. $\mathcal{F} = [V^{nom} - \beta, V^{nom} + \beta]$ represents the voltage feasible state. In brackets we describe the condition under which the transition will occur. In red we describe the action associated with the transition. In green we describe the properties of the state.

Third, the voltage penalty term depends on the state:

$$J_{V,k}(V_k) = \begin{cases} J_{A,k}(V_k) & \text{if bus } k \text{ in state I, II or III} \\ J_{B,k}(V_k) & \text{if bus } k \text{ in state IV,} \end{cases}$$

where $J_{A,k}$ and $J_{B,k}$ are defined next. $J_{A,k}$ enforces the hard constraint in Eq. (4), and has a fast increasing gradient outside the region $(V_k^{nom} - \beta_k + \epsilon, V_k^{nom} + \beta_k - \epsilon)$, where $\epsilon > 0$ is a safety margin. This has the effect that voltage remains in the safe region $(V_k^{nom} - \beta_k, V_k^{nom} + \beta_k)$ when there is no power step and an occasional excursion outside the safe region is allowed when there is a power step. $J_{B,k}$ differs from $J_{A,k}$ in that it has a dramatically larger gradient outside the safe region, so that the voltage quickly returns to it (see Fig. 2).

We now give the description of $J_{A,k}$ and $J_{B,k}$. Note that we impose $J_{A,k}$ and $J_{B,k}$ to have continuous gradients in order to avoid oscillations, which explains some of the complexities of the definitions below.

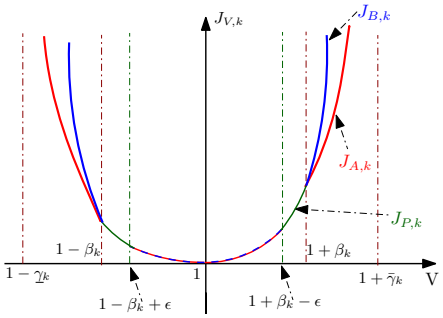

Fig. 2: Functions $J_{A,k}(V)$ and $J_{B,k}(V)$, $\alpha = 10^4$ and $V_k^{nom} = 1$.

First, we define $F_k(V, \mu)$ by:

$$F_k(V,\mu) = \frac{(V - V_k^{nom})^2}{\mu^2 - (V - V_k^{nom})^2} \tag{5}$$

Note that F_k is the function that was used in the Eq. (2). Second, we define the function $J_{P,k}(V)$ by:

1) defined on $[V_k^{nom} + \beta_k - \epsilon, V_k^{nom} + \beta_k]$ as the unique quadratic function that satisfies
   a) $\nabla_V J_{P,k}(V_k^{nom}+\beta_k-\epsilon) = \nabla_V F_k(V_k^{nom}+\beta_k-\epsilon, \bar{\gamma_k})$
   b) $\nabla_V J_{P,k}(V_k^{nom} + \beta_k) = \alpha \nabla_V F_k(V_k^{nom} + \beta_k, \bar{\gamma_k})$
   c) $J_{P,k}(V_k^{nom} + \beta_k - \epsilon) = F_k(V_k^{nom} + \beta_k - \epsilon, \bar{\gamma_k})$
2) defined on $[V_k^{nom} - \beta_k, V_k^{nom} - \beta_k + \epsilon]$ as the unique quadratic function that satisfies
   a) $\nabla_V J_{P,k}(V_k^{nom}-\beta_k+\epsilon) = \nabla_V F_k(V_k^{nom}-\beta_k+\epsilon, \underline{\gamma_k})$
   b) $\nabla_V J_{P,k}(V_k^{nom} - \beta_k) = \alpha \nabla_V F_k(V_k^{nom} - \beta_k, \underline{\gamma_k})$
   c) $J_{P,k}(V_k^{nom} - \beta_k + \epsilon) = F_k(V_k^{nom} - \beta_k + \epsilon, \underline{\gamma_k})$

where α is a very large parameter (= 10^4 in our case).

Third we introduce the functions $C_{1,k}(V)$ and $C_{2,k}(V)$. $C_{1,k}(V)$ is defined on $[V_k^{nom} + \beta_k, V_k^{nom} + \bar{\gamma_k}]$ as the unique linear function with the following properties:

1) $\nabla_V F_k(V_k^{nom} + \beta_k, \bar{\gamma_k}) + \nabla_V C_{1,k} = \nabla_V J_{P,k}(V_k^{nom} + \beta_k)$
2) $F_k(V_k^{nom}+\beta_k, \bar{\gamma_k}) + C_{1,k}(V_k^{nom}+\beta_k) = J_{P,k}(V_k^{nom}+\beta_k)$.

$C_{2,k}(V)$ is defined on $[V_k^{nom} - \bar{\gamma_k}, V_k^{nom} - \beta_k]$ as the unique linear function with the following properties:

1) $\nabla_V F_k(V_k^{nom} - \beta_k, \underline{\gamma_k}) + \nabla_V C_{2,k} = \nabla_V J_{P,k}(V_k^{nom} - \beta_k)$
2) $F_k(V_k^{nom}-\beta_k, \bar{\gamma_k}) + C_{2,k}(V_k^{nom}-\beta_k) = J_{P,k}(V_k^{nom}-\beta_k)$.

Now we can define $J_{A,k}$ as follows:

$$J_{A,k}(V) = \begin{cases} F_k(V, \bar{\gamma_k}) + C_{1,k}(V) & \text{if } V \in [V_k^{nom} + \beta_k, V_k^{nom} + \bar{\gamma_k}] \\ J_{P,k}(V) & \text{if } V \in [V_k^{nom} + \beta_k - \epsilon, V_k^{nom} + \beta_k] \\ F_k(V, \bar{\gamma_k}) & \text{if } V \in [V_k^{nom}, V_k^{nom} + \beta_k - \epsilon] \\ F_k(V, \underline{\gamma_k}) & \text{if } V \in [V_k^{nom} - \beta_k + \epsilon, V_k^{nom}] \\ J_{P,k}(V) & \text{if } V \in [V_k^{nom} - \beta_k, V_k^{nom} - \beta_k + \epsilon] \\ F_k(V, \underline{\gamma_k}) + C_{2,k}(V) & \text{if } V \in [V_k^{nom} - \underline{\gamma_k}, V_k^{nom} - \beta_k] \\ \infty & \text{otherwise.} \end{cases}$$

In other words, $J_{A,k}$ is given by the function F_k inside $(V_k^{nom}-\beta_k+\epsilon, V_k^{nom}+\beta_k-\epsilon)$, by the function F_k plus a large linear function outside the region $(V_k^{nom} - \beta_k, V_k^{nom} + \beta_k)$, and is patched between the two by means of $J_{P,k}$ such that it has a continuous derivative. Last, $J_{B,k}$ is defined by

$$J_{B,k}(V) = \begin{cases} \alpha J_{A,k}(V) - (\alpha - 1) J_{A,k}(V_k^{nom} + \beta_k) \\ \quad \text{if } V \geq V_k^{nom} + \beta_k \\ J_{A,k}(V) \\ \quad \text{if } V \in [V_k^{nom} - \beta_k, V_k^{nom} + \beta_k] \\ \alpha J_{A,k}(V) - (\alpha - 1) J_{A,k}(V_k^{nom} - \beta_k) \\ \quad \text{if } V \leq V_k^{nom} - \beta_k. \end{cases}$$

We next show how the algorithm handles overvoltages. The idea is schematically illustrated on Fig. 3 for a possible voltage trajectory (with $\beta_k = 0.1$ and $\bar{\gamma_k} = 0.2$). The trajectory starts with no violation. Then, at time t_1 a violation of the $V_k^{nom}+\beta_k$ bound occurs, and $\tau_{v,k}$ starts counting; at time t_2 the voltage goes back below the bounds and $\tau_{r,k}$ starts counting. Note that, at this stage, the violation is still allowed, since $\tau_{v,k}$ has not elapsed. Finally, at time t_3 the violation period ends.

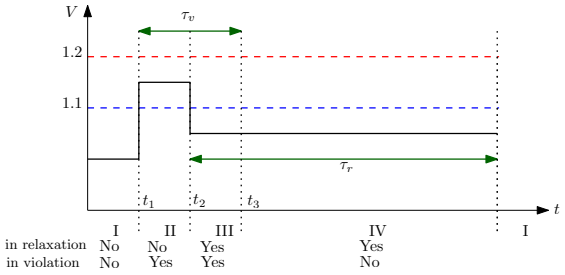

Fig. 3: Voltage trajectory with time period dynamics.

B. Modification to the Current Penalty-Function

In the case of the current penalty function, we propose a method to track the thermal limit I_l^{max}, and we propose a new definition for the current penalty-function. For the first, we rely on the fact that the operational limit of a conductor is its maximum temperature, which will be reached at different speed depending on the magnitude of the transferred current. We consider the energy balance equation of a conductor [6],

$$RI^2 = mc_p\dot{\theta}(t) + k_t S(\theta(t) - \theta_a), \tag{6}$$

where θ_a is the ambient temperature, I is the current magnitude and θ the conductor's temperature, while R, m, c_p, k_t and S are physical parameters of the conductor (the per-unit-length resistance of the conductor [Ω/m], the per-unit-length mass of the cable insulator [kg/m], the specific heat of the insulator [J/(kg°C)] and the global heat-exchange coefficient of the cable [W/(m^2°C)] respectively). The three elements of the equation represent: Joule losses, heat capacity and forced convection respectively. We assume that all other sources of heating or cooling are negligible (e.g. solar radiation, radiated heat, etc.). In practice, many of the parameters of Eq. (6) are difficult to find in datasheets and the temperature estimation through a model becomes an untractable problem.

Instead, we propose to re-write Eq. (6) as

$$(\theta_m - \theta_a) I/\bar{I} = H/\bar{I}^2 \dot{\theta}(t) + (\theta(t) - \theta_a), \tag{7}$$

where θ_m is the maximum temperature, $\overline{I}$ is the ampacity and H is the *heat impulse*[4] (in A^2s) of the conductor. These three parameters are typically found in cables datasheets.

In practice, Eq. (7) represents the time to reach the maximum temperature for a given current magnitude. Indeed, when the current magnitude is below the ampacity the conductor can operate forever since $\theta|_{t=\infty} < \theta_m$, while the time will be finite only for values above the ampacity. The current-dependent energy involved in this process is known as the *specific energy* (in A^2s). This suggests that, in general, the conductor has an energy *quota* that is only used for values larger than the ampacity. This definition follows the IEC standard [2], that bounds the loss of insulation life of the cable per overload. To account for this use, we continuously evaluate the *integral of Joule* i_J, that represents a state, using

$$i_J[k] = \begin{cases} i_J[k-1] + I[k]^2 \Delta t & \text{if } I > \overline{I}, \\ i_J[k-1] e^{-\Delta t/\tau_I} & \text{if } I < (1-\epsilon_I)\overline{I}, \\ i_J[k-1] & \text{otherwise,} \end{cases} \quad (8)$$

where I is the current magnitude, Δt the time spent between time-steps $k-1$ and k, $\epsilon_I > 0$ and $\tau_I = H/\overline{I}^2$ represents the decay time-constant of Eq. (7). Using this state, the maximum allowed current magnitude I^{max} is the solution of

$$I^2 \Delta \hat{t} = -H/\overline{I}^2 \ln(1 - (\overline{I}/I)^2) I^2 - i_J, \quad (9)$$

where $\Delta \hat{t}$ is the estimation of the time that current I will be implemented. The equation cannot be solved analytically. It is solvable, instead, numerically using a lookup-table approach, compatible with the real-time operation. In order to account for the temporal reduction of the maximum allowed current, we propose the following penalty function

$$J_I = \sum_l \frac{\left(\frac{I_l^*}{I_l^{max}}\right)^2 I_l^2}{(I_l^*)^2 - I_l^2},$$

where I_l^* is the maximum allowed current when $i_J = 0$ for $\Delta \hat{t}$, that is used as a hard constraint.

IV. Validation

We evaluate the proposed method using both simulation and an implementation in a real-scale microgrid. In this paper we give results obtained by simulation and results from the implementation in the real-scale microgrid (see Fig. 6).

A. Simulation Scenario

Our simulation setup consists of the following elements: a battery (B), an electric vehicle (EV) and a photovoltaic plant (PV). The PV is uncontrollable and is characterized by a rated power of 20kW. It is assumed that the PV injects only active power. The EV, assumed to behave as an uncontrollable load, constantly consumes 30kW (P_{max}). The battery in our case is considered as a fully controllable device and its rated power 25kW. We assume that the battery is almost charged (90%) at the beginning and has a long-term objective to get discharged. For both battery and PV plant the PQ profile, virtual cost and belief function are adopted from [5].

Our goal is to simulate a sudden disconnection of the EV. For that reason we assume that initially the EV active power is $-P_{max}$ and it suddenly goes to zero (at time t_2). As the resource cannot be controlled, we define the PQ profile as the actual measured active-power, the virtual cost equals to zero and the BF will express the power change uncertainty. At the beginning of the simulation, the EV agent advertises a small belief set $[-P_{max}, -P_{max}+\delta]$[5]. At time t_1, as the agent predicts that the EV may get disconnected, it will advertise the belief set $[-P_{max}, 0]$. In this specific scenario, we use small bounds for the voltage and current constraints, so that they are replicable in the real-scale microgrid.

B. Simulation Results: Voltage Violation

For the validation of the proposed method, we present two cases: *case 1* using the GA as described in [4] and *case 2* with the proposed method integrating the new voltage penalty. The simulation results are shown in Fig. 4, that shows the battery power and the voltage profile of the bus where the EV is connected. Note that, at the beginning of the simulation, the GA in both cases behaves similarly as expected. That is, the battery is allowed to provide the same amount of active power. However, at time t_1 the EV agent expands its belief function. The GA of case 1 will try to prevent the worst-possible scenario, namely, a large voltage-step caused by a sudden EV disconnection, before it happens. Since in our setup the only controllable device is the battery, the GA, in a conservative action, reduces the battery production. On the contrary, the GA of case 2 will continue allowing the battery to produce power. We also shown that, when the EV actually disconnects (at time t_2), the voltage does not exceed the smaller bound, in case 1. In case 2, the GA reduces the power production of the battery and brings the voltage back to the safe region after the allowed violation period ends at time t_3.

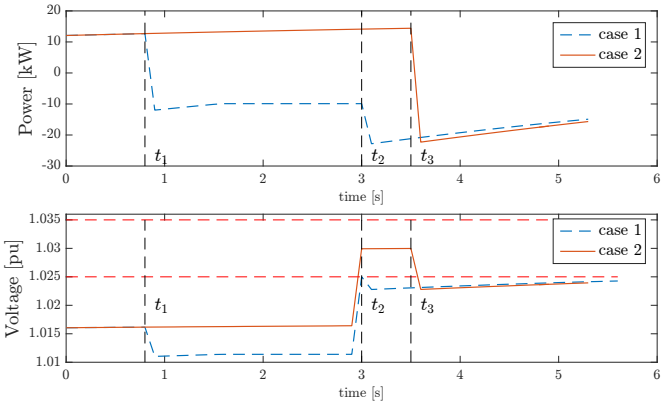

Fig. 4: Simulation results for the voltage violation case.

[4]Where $H = \frac{mc_p}{R}(\theta_m - \theta_0)$, and θ_0 is the initial conductor-temperature.

[5]Negative power indicates consumption. We take δ = 10% of P_{max}

C. Simulation Results: Current Violation

We present in Fig. 5 the evolution in time of the current in a congested line, the state variable i_J of the same line and the active power of the battery. Before t_2, the power of the battery slightly decreases. When the EV is disconnected, the lines gets congested and i_J of the line of interest quickly increases. Consequently, the dynamic current limit I_l^{max} decreases, forcing the actual flowing current magnitude to decrease as well. When the current magnitude goes below $(1-\epsilon_I)\overline{I}$, i_J decreases exponentially letting the battery to increase the power back[6].

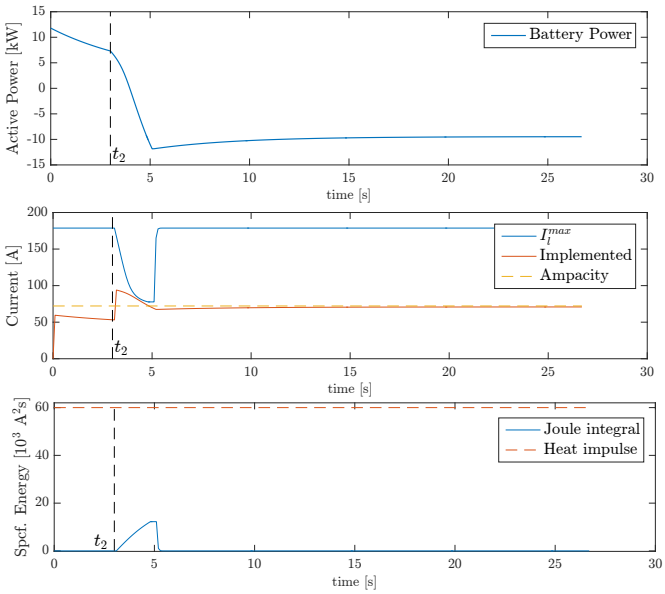

Fig. 5: Simulation results for the current violation case.

D. Experimental Setup

The results described in this section refer to the application of the proposed methodology to a real-scale microgrid, that represents at real-scale the CIGRÉ low-voltage (400V at 50Hz) microgrid benchmark defined in [7]. For simplicity, we only use a subset of the energy resources: a controllable resource (L1), a battery (B) and a photovoltaic plant (PVR). L1 is a fully controllable 4-quadrants resource, that is used in this case for creating the power step.

The microgrid of Fig. 6 is connected to a 20kV grid at bus B01 via a suitable transformer. The line that connects to the transformer, L01, has a current limit of 40A, i.e. a power transfer limit of ca. 28kVA.

E. Experimental Results: Voltage Violation

Since our experimental setup (see Fig. 6) does not have a real EV, we use the controllable resource L1 instead, in order to emulate a large power step. In this section, we present the behavior of the voltage at the node where L1 is located (B03) when a large power step of 30kW is produced by L1.

At the beginning of the experiment, L1 consumes 15kW. Then, we emulate the power step by producing 15kW with it.

[6]We take $\epsilon_I = 0.1$.

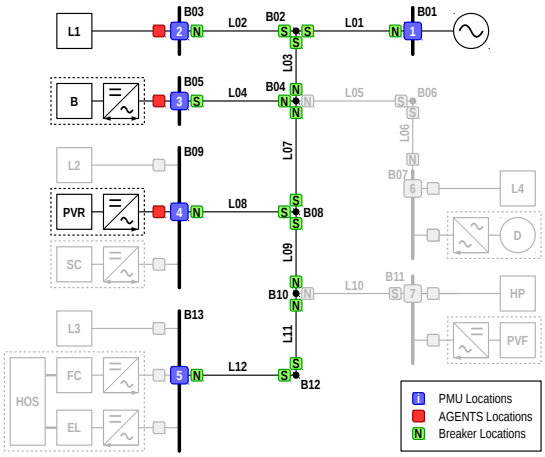

Fig. 6: The experimental microgrid. In black all elements participating in this paper's experiments. Location of measurement devices for state estimation (PMUs) are also indicated.

This 30kW power step causes a violation of $\beta = 4\%$ of the nominal voltage. In Fig. 7 we show how the GA reduces the power production of the battery and brings the voltage of node B03 back to the safe region after the allowed violation period ends. Also, it is interesting to see that due to the definition of J_P, the voltage stabilizes below its soft limit β.

F. Experimental Results: Current Violation

In this section, we focus on the behavior of the current of line L01 when a large power step of 20kW is produced by the sudden increment of L1. The emulated load has a power factor of 0.9, thus the reactive power consumption also increases accordingly. In this specific scenario, we have considered that the PV is not injecting power into the microgrid and that the battery is being charged. In Figure 8 we show how the proposed methodology allows an initial current violation, that triggers the increment of the line's integral of Joule i_J. Consequently, after solving Eq. (9), the maximum allowed current I_l^{max} decreases, forcing the GA to quickly steer the battery power to reduce the current at L01. When the current magnitude reaches safe values, i_J smoothly decreases following Eq. (8). This smooth behavior permits that the current I_l stabilizes at safe values even when the perturbation is persistent.

V. Conclusions

In this paper we have proposed a method by which a microgrid real-time control can handle large power steps by allowing and controlling temporary voltage and current violations so that they remain within the limits imposed by standards and safe operation. This brings more flexibility to the grid operation, which can lead to better operational results such as increased self-consumption or higher EV charging rates. The proposed methodology has been validated both with simulations and experimentally.

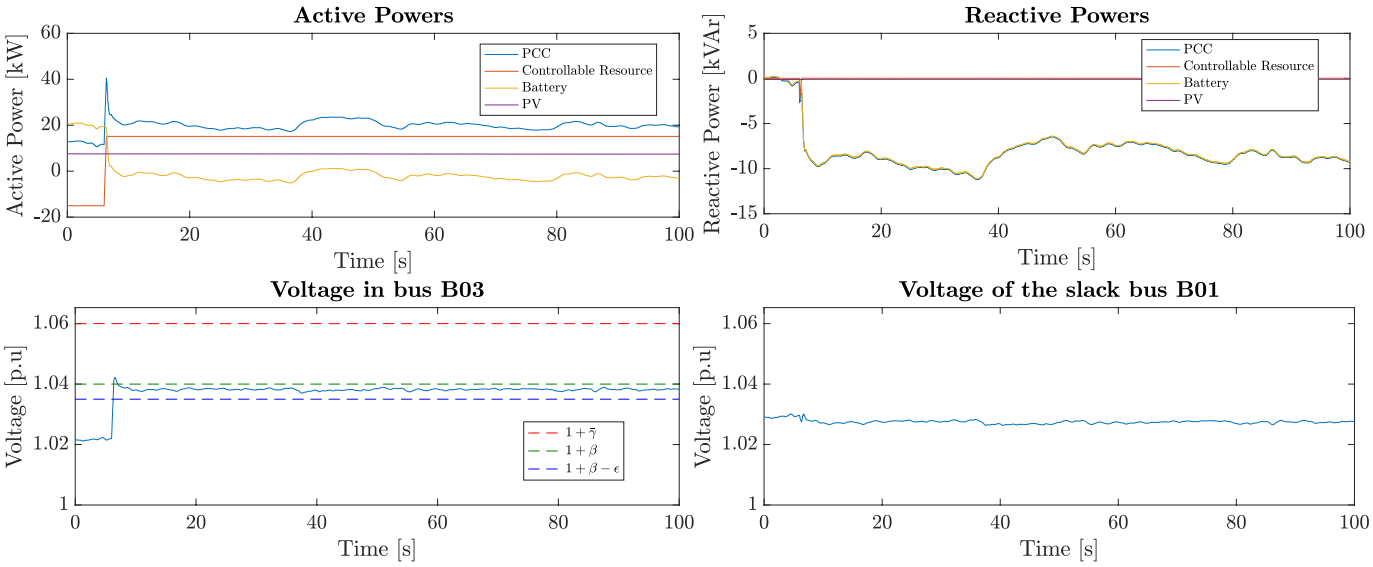

Fig. 7: Experimental results for the voltage violation case.

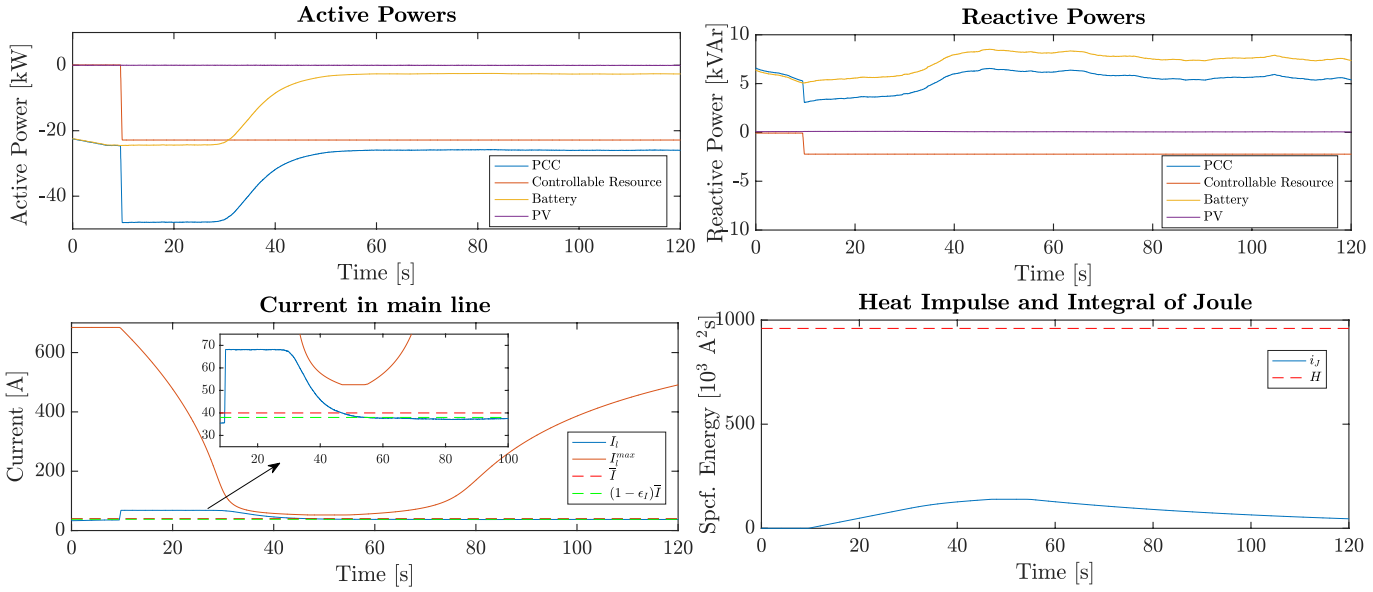

Fig. 8: Experimental results for the current violation case. The plots in the lower part refer to line L01 of Fig.6.

REFERENCES

[1] IEEE Power and Energy Society, "IEEE Guide for Voltage Sag Indices," 2014.

[2] International Electrotechnical Commission, "International Standard: Electric cables – calculation of the current rating," 2007.

[3] IEEE Power Engineering Society, "IEEE Standard for Calculating the Current-Temperature of Bare Overhead Conductors," 2006.

[4] A. Bernstein, L. Reyes-Chamorro, J.-Y. Le Boudec, and M. Paolone, "A composable method for real-time control of active distribution networks with explicit power set points. Part I: Framework," *Electric Power Systems Research*, vol. 6, no. August, pp. 254–264, 2015.

[5] L. Reyes-Chamorro, A. Bernstein, J.-Y. Le Boudec, and M. Paolone, "A composable method for real-time control of active distribution networks with explicit power set points. Part II: Implementation and validation," *Electric Power Systems Research*, vol. 6, no. August, pp. 265–280, 2015.

[6] J. Snajdr, J. Sedláček, and Z. Vostracký, "Application of a line ampacity model and its use in transmission line operations," *Journal of Electrical Engineering*, vol. 65, no. 4, pp. 221–227, 2014.

[7] S. Papathanassiou, N. Hatziargyriou, and K. Strunz, "A benchmark low voltage microgrid network," in *Proceedings of the CIGRÉ Symposium "Power Systems with Dispersed Generation: technologies, impacts on development, operation and performances"*, Apr. 2005, Athens, Greece.